Quantitative Prediction of Multivalent Ligand-Receptor Binding Affinities for Influenza, Cholera and Anthrax Inhibition

Susanne Liese [1,2] and Roland R. Netz [1*]

[1]Freie Universität Berlin, Department of Physics, 14195 Berlin, Germany

[2]University of Oslo, Department of Mathematics, 0851 Oslo, Norway

[*]Email: rnetz@physik.fu-berlin.de

Abstract

Multivalency achieves strong, yet reversible binding by the simultaneous formation of multiple weak bonds. It is a key interaction principle in biology and promising for the synthesis of high-affinity inhibitors of pathogens. We present a molecular model for the binding affinity of synthetic multivalent ligands onto multivalent receptors consisting of n receptor units arranged on a regular polygon. Ligands consist of a geometrically matching rigid polygonal core to which monovalent ligand units are attached *via* flexible linker polymers, closely mimicking existing experimental designs. The calculated binding affinities quantitatively agree with experimental studies for cholera toxin ($n = 5$) and anthrax receptor ($n = 7$) and allow to predict optimal core size and optimal linker length. Maximal binding affinity is achieved for a core that matches the receptor size and for linkers that have an equilibrium end-to-end distance that is slightly longer than the geometric separation between ligand core and receptor sites. Linkers that are longer than optimal are much preferable compared to shorter linkers. The angular steric restriction between ligand unit and linker polymer is shown to be a key parameter. We construct an enhancement diagram that quantifies the multivalent binding affinity compared to monovalent ligands. We conclude that multivalent ligands against influenza viral hemagglutinin ($n = 3$), cholera toxin ($n = 5$) and anthrax receptor ($n = 7$) can outperform monovalent ligands only for a monovalent ligand affinity that exceeds a core-size dependent threshold value. Thus multivalent drug design needs to balance core size, linker length as well as monovalent ligand unit affinity.

KEYWORDS: multivalency, binding affinity, pathogen inhibition, statistical mechanics modeling

Multivalent interactions appear in a wide range of biological processes, including cell signaling,[1,2] protein recognition,[3–5] and cell adhesion.[6,7] Multivalency describes the simultaneous binding be-

tween several monovalent ligand and receptor units.[3,8] Nature employs multivalency to enhance the binding affinity of weakly binding moieties, such as lectins, which are proteins that interact with carbohydrates.[9,10] The potential of multivalency is best illustrated by considering the dissociation constant of a specific lectin-carbohydrate pair, such as hemagglutinin and sialic acid. Hemagglutinin, a trimeric lectin on the influenza virus surface, mediates the contact between virus and host cell by binding to sialic acid, a sugar moiety covering epithelial cells.[11] Each influenza virus carries up to 1000 hemagglutinin proteins. Sialic acid ligands are expressed with a surface density of 0.5-2 per nm^2 on the host cell.[12] The dissociation constant for monomeric hemagglutinin and sialic acid is around K_1=2.5mM,[13] which is a typical value for lectines.[14] In contrast, the dissociation constant between the entire virus and a host cell is estimated to lie in the pM range.[12] Thus the binding affinity, the inverse of the dissociation constant, increases by nine orders of magnitude, which strikingly illustrates the potency of multivalent interactions. Furthermore, it has been shown that a slight variation of the monovalent dissociation constant K_1 between hemagglutinin and a ligand molecule leads to an order of magnitude improvement of the multivalent binding affinity, which is employed by nature to achieve strain selective binding.[11,15] In fact, the binding enhancement of multivalent ligands has been theoretically and experimentally shown to superselectively depend on the receptor surface concentration.[16,17] In efforts to utilize similar principles for the synthesis of drugs against pathogens, in recent years multivalent ligand synthesis has moved into the focus of attention.[8,18,19] Pharmacological studies on low-molecular-weight vaccines and inhibitors with tailored valency, size and molecular flexibility have been conducted.[10,20] Typical synthetic multivalent ligands consist of rigid cores of different chemical composition to which ligand units are attached *via* flexible polymeric linkers.[3,18,21,22] Multiple structural parameters, such as size and shape of the core, as well as the linker length, together with costly and time-consuming synthesis procedures, call for quantitative models that aid in the affinity optimization of such multivalent ligands.

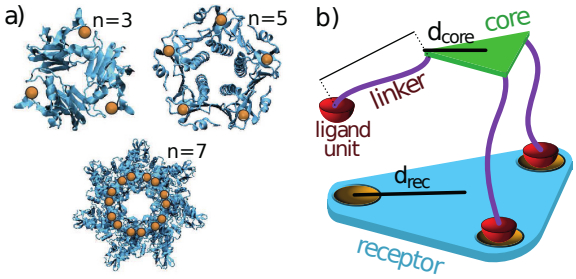

Figure 1: **Multivalent ligand-receptor complexes:** a) Structures of the multivalent receptors considered in this paper: Hemagglutinin (n = 3, pdb-entry: 1hgg), Cholera toxin (n = 5, pdb-entry: 1lta), Anthrax (n = 7, pdb-entry: 1tzo). The protein structure is shown in blue, the receptor binding pockets are visualized by orange spheres. b) Our model for a trivalent ligand consists of three ligand units which are attached to a rigid core *via* flexible, polymeric linkers.

In Fig. 1a three prominent pathogen examples are shown: trivalent hemagglutinin, pentavalent cholera toxin and the heptavalent anthrax receptor. As mentioned above, hemagglutinin plays a crucial role in influenza infections. Influenza causes up to 500 000 deaths every year,[23] which illustrates the need for efficient anti-influenza drugs. So far, no drug targets the sialic acid binding receptor,[24] one reason being the above-mentioned large monovalent dissociation constant of K_1=2.5mM.[12] Here, multivalent ligands hold high potential to improve the binding affinity.[17,25,26] An even greater health risk is posed by cholera and anthrax, which involve the attachment of the pentavalent cholera toxin and the heptavalent anthrax receptor to cells, respectively. Zhang *et al.*[27,28] and Joshi *et al.*[29] have developed geometrically matching ligands which will be discussed in detail further below. In both studies monovalent ligand units were attached to rigid cores *via* flexible polymeric linkers. Joshi *et al.* investigated the influence of linker length on the dissociation constant of a heptavalent ligand against the anthrax receptor for a single core size (results for the dissociation constant are shown as symbols in Fig.4a), while Zhang *et al.* varied core size as well as linker length of a pentavalent ligand against the cholera toxin (results are shown as symbols in Fig.4b).

In the present paper we derive an analytically tractable theoretical model for the binding affinity between multivalent ligand-receptor pairs. Our main aim is to derive explicit guidelines for the rational ligand design in terms of structural ligand parameters. Our focus is on receptors with binding pockets arranged on a regular polygon, as found for a wide range of biologically relevant receptors. We restrict the model to ligands that have the same valency as the receptor, which is the typical experimental situation. In previous works we and others investigated the impact of linker flexibility on the binding affinity of divalent ligands.[30–32] Here we extend these models to ligands of higher valencies which adds considerable complexity to the theory. Our model results, presented by lines in Fig.4 a and b, successfully reproduce both experiments. Beyond this validation, we study the binding affinity for varying core size and find that the strongest binding is achieved for a core size d_{core} that matches the receptor size d_{rec}. We also investigate the robustness of the binding affinity with respect to variations of the linker length and find that ligand constructs with an optimal core size require a precise choice of the linker length: linkers that are longer than optimal are much preferable compared to linkers that are shorter than optimal. Our model identifies the angular steric restriction between ligand units and linker chains as an important parameter that significantly influences the multivalent binding affinity. Finally, we establish an enhancement diagram based on parameter combinations for which a multivalent ligand binds more efficiently – compared with the monovalent ligand unit – onto a multivalent receptor. The monovalent ligand-receptor dissociation constant K_1 here plays a key role: for given ligand core size and linker length, a multivalent ligand can only beat the monovalent ligand if K_1 is smaller than a critical value, which is an important message for the design of synthetic ligand constructs.

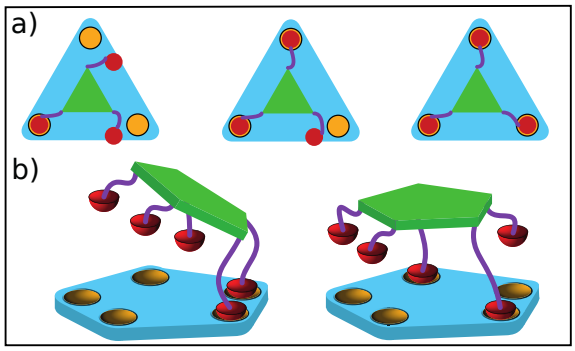

Figure 2: **Multivalent binding modes:** a) A trivalent ligand-receptor pair exhibits three binding modes with one, two or three ligand units (red spheres) bound to the receptor pockets. b) A pentavalent ligand with two bound ligand units exhibits two different binding patterns.

Results and Discussion

Multivalent Binding Affinity: The geometric parameters that characterize a multivalent ligand receptor pair are visualized in Fig. 1b for the example of a trivalent receptor that interacts with the corresponding ligand. The monovalent ligand units (red half spheres) are attached to the core (green triangle) *via* flexible polymeric linkers that in experiments consist of polyethylene glycol (PEG) or peptides.[25,33] The linker length is parameterized by the unperturbed average end-to-end distance $r_{\rm ete}$. The distance from the ligand core midpoint to the corner is denoted as $d_{\rm core}$. Similarly, the distance between the receptor midpoint and the corner is denoted as $d_{\rm rec}$. The binding between n-valent ligands L and receptors R is described by the chemical reaction

$$L + R \rightleftharpoons LR. \tag{1}$$

The n-valent dissociation constant $K_{\rm n}$ is defined as

$$K_{\rm n} = \frac{[L][R]}{[LR]}, \tag{2}$$

where $[L]$ is the concentration of free n-valent ligands, $[R]$ is the concentration of free n-valent receptors, and $[LR]$ is the concentration of bound receptor-ligand pairs. The experimental key quantity of interest is the half-maximal inhibitory concentration IC_{50}, which is typically defined as the total ligand unit concentration at which half of all receptors are bound to a ligand, so that $[R] = [LR]$ and thus $K_{\rm n} = [L]_{50}$. In the limit of dilute receptors we have $[L]_{tot} = [L] + [LR] \approx [L]$ and so $IC_{50} = n[L]_{50} = nK_{\rm n}$. We thus see that the dissociation constant $K_{\rm n}$ serves as an inverse measure of the inhibitory efficiency of a ligand. Obviously, the main aim of multivalent ligand design is to minimize the dissociation constant $K_{\rm n}$. The definition of a bound ligand-receptor complex deserves some discussion, since an n-valent ligand can bind onto an n-valent receptor in n distinct modes that are distinguished by the number of bound ligand-receptor units, as shown for a trivalent ligand in Fig.2a. In addition, for ligands with valency $n > 3$ there are different

binding patterns for a given number of bound ligand units that have to be accounted for, as shown in Fig.2b for a pentavalent ligand with two bound ligand units. One choice is to define a ligand to be bound to a receptor when at least one ligand unit is attached to a receptor. This choice is suitable for competitive inhibition assays where the host-pathogen binding is probed and presumably also relevant *in vivo*.[12,34] As shown in the Supporting Information (Fig. S5), for the systems investigated here, the dominant contribution to the multivalent binding affinity comes from the binding mode where all n ligand units are bound; taking also partially bound ligands into account alters the dissociation constant by not more than a factor of two. Since the aim of multivalent ligand design is to decrease the dissociation constant by several orders of magnitude, we consider this deviation negligible. Accordingly, we define a ligand-receptor pair to be bound when all n ligand units are bound to the receptor, in which case K_{n} can be expressed as

$$K_{\mathrm{n}} = \frac{K_1^n \omega_{\mathrm{LU}}^n}{m^n C_{\mathrm{n}}}. \tag{3}$$

A detailed derivation of Eq. 3 is given in the Supporting Information. We distinguish four contributions: (1) The dissociation constant of the monovalent ligand unit K_1. (2) The angular steric restriction between ligand unit and linker chain ω_{LU} (which will be explained below). (3) The number of binding pockets per receptor subunit m, which is m=1 for hemagglutinin and cholera toxin and m=2 for the anthrax receptor, as depicted in Fig.1a. (4) The cooperativity factor C_{n}. While the effects of K_1, ω_{LU} and m factorize and hence enter Eq. 3 with a power of n, all non-factorizing effects are contained in C_{n}.

Cooperativity Factor: C_{n} describes the conditional probability that if a single ligand unit is bound to a receptor unit, the other $n-1$ ligand units are located in receptor pockets as well. Accordingly, it has units of concentration to the power n-1 and generalizes the concept of an effective concentration introduced for divalent ligands.[35] It follows from the integral over the position and angular orientation of the ligand core and the conformational integrals over all linker chains, while taking into account that the linker chains cannot penetrate into the receptor surface. In our model, we approximate the linker polymer distribution as Gaussian and neglect steric repulsion among linker chains and between linker chains and the ligand core. The detailed calculation together with a closed-form approximation for C_{n} is presented in the Supporting Information.

Angular restriction factor ω_{LU}: We first discuss the impact of ligand angular restrictions for a monovalent ligand unit. The monovalent dissociation constant K_1 is proportional to an angular contribution that can be written as

$$K_1 \sim \frac{8\pi^2}{\Omega_{\mathrm{bp}}}, \tag{4}$$

where $8\pi^2$ is the angular space of an unconstrained rigid body, which is the product of the orientational space of a vector (corresponding to the area of a unit sphere 4π) times a factor 2π for rotations around the body axis. The angular space available to a ligand that is bound within a receptor binding pocket is, due to interactions between ligand and receptor, reduced to Ω_{bp}, with

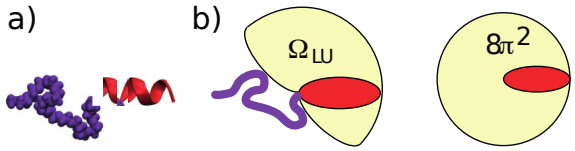

Figure 3: **Angular restriction factor:** a) Schematic picture (drawn to scale) of the ligand unit that in the experimental study binds to the anthrax receptor, consisting of a helical peptide connected to a PEG linker with N=15 monomers.[29] b) Visualization of the angular restriction of the ligand relative to the linker chain (left) compared to the free ligand (right).

$0 < \Omega_{\rm bp} < 8\pi^2$, which can give a sizable contribution to K_1. If the ligand unit is bound to a linker chain, the available angular space of the ligand unit $\Omega_{\rm LU}$ relative to the orientation of the linker chain, which is approximately given by the linker end-to-end vector, will be reduced due to steric effects. We illustrate this angular steric repulsion in Fig. 3 where we draw the alpha-helical peptide ligand unit with amino-acid sequence HTSTYWWLDGAP, which has a length of roughly 1.5nm, connected to a PEG linker with N=15 monomers, which is the ligand-linker construct actually used to block the anthrax receptor.[29] The PEG structure is a typical conformation from an MD simulation[36] and linker and ligand are drawn to scale. If we assume the linker chain in the bound complex to be oriented perpendicularly to the receptor surface, the reduction of angular space due to binding of the ligand unit into the binding pocket is not $8\pi^2/\Omega_{\rm bp}$, as for a monovalent ligand, but rather $\Omega_{\rm LU}/\Omega_{\rm bp}$. Hence, we have to correct the monovalent binding constant K_1 by a factor $\omega_{\rm LU} = \Omega_{\rm LU}/8\pi^2$ per bound ligand unit, which leads to the factor $\omega_{\rm LU}^n$ in Eq. 3. In other words, the more the orientation of the ligand unit is restricted, *i.e.* the smaller $\omega_{\rm LU}$, the more the multivalent dissociation constant $K_{\rm n}$ is reduced. In the comparison with experimental data, $\omega_{\rm LU}$ is the only fitting parameter. We note that due to the fitting to experimental data, $\omega_{\rm LU}$ will also account for other effects that modify the monovalent binding affinity and that are not accounted for in our model, such as linker adsorption onto the receptor surface. A detailed discussion of the relation between our model assumptions and the resulting fit value for $\omega_{\rm LU}$ is given in the Supporting Information.

Linker-Length Influence: Joshi *et al.* synthesized a heptavalent ligand (schematically shown in Fig.4c) based on seven alpha-helical peptide ligand units (shown in Fig.3a), which binds to the anthrax receptor.[29] The ligand core consists of cyclodextrin (Fig.4c). The PEG linker length is varied between N=2 to N=27 monomers. By mutation studies of the receptor each of the seven receptor subunits was found to exhibit two binding pockets[29] as indicated in Fig.1a. The anthrax receptors were pre-incubated with the lethal factor and the heptavalent ligands and afterwards the cytotoxicity towards RAW264.7 cells was measured. In the experiment, the ligand unit concentration $\rm IC_{50}$ required to inhibit cytotoxicity by 50% was determined, in Fig.4a we show the multivalent dissociation constant $K_7 = IC_{50}/7$ as open spheres in dependence of the linker length $r_{\rm ete}$. For ligands with short linkers $r_{\rm ete}$ $\leq$1.05nm the cytotoxicity inhibition was not measurable

for ligand unit concentrations of up to 10^{-5}M, which is indicated by crosses. We calculate r_{ete} from the ideal scaling expression

$$r_{\mathrm{ete}} = \sqrt{b \cdot a_0} \cdot \sqrt{N-1} \tag{5}$$

where the Kuhn length b=0.68nm and the monomer length a_0=0.356nm for PEG have been determined previously in MD simulations.[36] The same simulations have also shown that the scaling law in Eq. 5 holds even for short ($N \leq$24) polymers.

The theoretical dissociation constant K_7 based on Eq. 3 is shown as a solid line in Fig.4a. For the monovalent ligand dissociation constant we use a value of K_1=2mM, which is reported as a lower limit.[29] The distance from the binding pocket to the receptor midpoint is determined from the anthrax receptor crystal structure (pdb-entry: 1tzo) as d_{rec}=3.5nm for both binding pockets, the core size of d_{core}=1.5nm is determined from the chemical structure of the ligand core shown in Fig.4c. The only free parameter in Eq.3 is the angular restriction factor which by a fit to the experimental data is given by $\omega_{\mathrm{LU}} = 0.06$. The importance of ω_{LU} becomes apparent by the plot of K_7 for the value $\omega_{\mathrm{LU}} = 1$ (dashed line in Fig.4a), which corresponds to the scenario where the ligand unit orientation is not influenced by the PEG linker: The dissociation constant K_7 is increased by more than seven orders of magnitude, since ω_{LU} enters Eq.3 as the seventh power. We note that changing the angular restriction factor ω_{LU} shifts the dissociation constant in Fig.4a vertically, while the position of the minimum, *i.e.* the optimal linker length, and the functional dependence of the dissociation constant on the linker length are not altered. Hence, the optimal linker length, which agrees nicely with the experimental value, is predicted in a parameter-free fashion by our model.

Zhang *et al.*[27,28] designed pentavalent ligands with four different core sizes that bind to the cholera toxin B pentamer, which recognizes the GM1 ganglioside on the cell surface. The ligand and receptor structures are schematically shown in Fig.4d. Galactose ligand units (indicated in red in Fig.4e and f) are attached to a pentavalent core (indicated in green in Fig.4e and f) *via* a polymeric linker, which is a heteropolymer of predominantly PEG units, as depicted in Fig.4e and f. To estimate the average linker end-to-end distance r_{ete}, we divide the number of backbone atoms by three to obtain an effective number of PEG monomers N. The average end-to-end distance r_{ete} is then calculated by Eq.5. From the crystal structure (pdb-entry: 1ilta) the receptor size is determined as d_{rec}=2.5nm. Experimentally a dissociation constant K_1=100mM was determined for monovalent galactose.[27] Attaching a short linker (N=1 in Fig.4f) to the monovalent galactose reduced the dissociation constant to K_1=5mM,[37] which suggests additional attractive interactions between the linker and the receptor, presumably due to the polar carbonyl group close to the galactose unit. Since the anchoring chemistry between galactose and the linker is the same for all pentavalent ligands, we use K_1=5mM for our calculations. The IC_{50} values are obtained from the attachment inhibition of cholera toxin to planar galactose-functionalized surfaces in an ELISA assay, from which the dissociation constant follows as $K_5 = IC_{50}/5$.

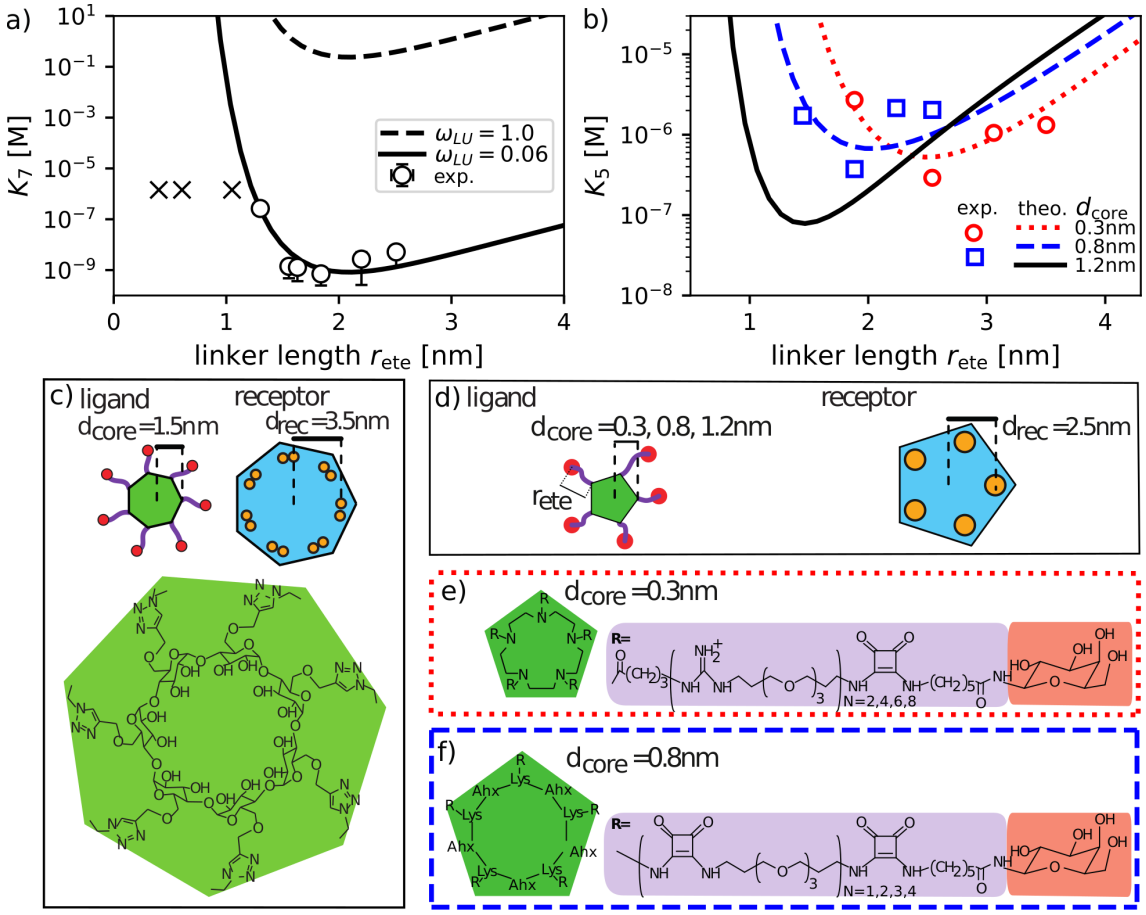

Figure 4: **Multivalent ligand-receptor complexes:** a) Dissociation constant K_7 of a heptavalent ligand that inhibits the anthrax receptor. Experimental data (spheres) from Ref.[29] are compared to Eq.3 (solid line) with a fitted angular restriction factor of $\omega_{LU} = 0.06$ (solid line) and $\omega_{LU} = 1$ (broken line). For linkers shorter than $r_{\rm ete} \leq$1.05nm the cytotoxicity inhibition was not measurable, the upper experimentally measurable limit is denoted by crosses. b) Experimental dissociation constant K_5 of pentavalent ligands with two different core sizes, which bind to cholera toxin. The simultaneous fit of Eq.3 with n=5 (lines) to the two experimental data sets[27,28] (data points) leads to $\omega_{LU} = 0.03$ (red dotted and blue broken lines). c) Chemical structure of the experimentally used heptavalent ligand core.[29] d) Schematic picture of the pentavalent ligand and receptor. e) Chemical structure of the pentavalent ligand with a core size of $d_{\rm core} = 0.3$nm. The corresponding theoretically predicted dissociation constant is shown as a red dotted line in subfigure b. f) Chemical structure of the pentavalent ligand with a core size of $d_{\rm core} = 0.8$nm. The corresponding theoretically predicted dissociation constant is shown as a blue dashed line in subfigure b.

In Fig.4b we compare experimental data for the smallest core size d_{core}=0.3 nm, consisting of acylated pentacyclen (shown in Fig.4e) and the largest core size d_{core}=0.8 nm, consisting of a cyclic peptide structure (shown in Fig.4f) with our model (dashed blue and red dotted lines). The angular restriction factor $\omega_{\text{LU}} = 0.03$ results from a simultaneous fit to both experimental data sets, the agreement with the experimental data is convincing. Not surprisingly, the optimal linker length (corresponding to a minimal value of K_5) is larger for the smaller core size. We also present the theoretical prediction for an even larger ligand core with d_{core}=1.2nm (black solid line in Fig.4b) for the same value $\omega_{\text{LU}} = 0.03$. The minimal dissociation constant K_5 is further reduced by an order of magnitude. We observe that the curvature of K_5 around the minima increases with increasing d_{core}, meaning that the robustness of the binding affinity with respect to variations of the linker length away from the optimal value decreases as the ligand core size is optimized; we will come back to this point later on. The dissociation constant K_5 as a function of d_{core} for fixed linker length is presented in the Supporting Information Fig. S7.

Core Size Influence: Fig.5a shows K_5 in dependence of the ligand core size d_{core} for the same parameters and in particular using the same fitted value for the angular restriction factor ω_{LU} as in Fig.4b for cholera toxin. As discussed before, changing the value of ω_{LU} shifts the dissociation constant by a constant factor, while the optimal linker length and core size remain unaltered. We present model predictions for the optimal linker length $r_{\text{ete}}^{\text{opt}}$ that minimizes K_5 (solid line) as well as for a linker that is shorter $r_{\text{ete}} = r_{\text{ete}}^{\text{opt}}-0.3$nm (dotted line) and longer $r_{\text{ete}} = r_{\text{ete}}^{\text{opt}}+0.3$nm (dashed line) than optimal. Not surprisingly, we see that the ligand is most efficient, which means K_5 is smallest, if the ligand core size is similar to the receptor size ($d_{\text{core}} = d_{\text{rec}}$ is denoted by a vertical broken line). In Fig.5b the optimal linker length $r_{\text{ete}}^{\text{opt}}$ is shown in dependence of d_{core} as a solid line. $r_{\text{ete}}^{\text{opt}}$ is slightly larger than the difference between receptor size and core size $|d_{\text{core}} - d_{\text{rec}}|$, denoted by broken straight lines. The right axis denotes the number of PEG monomers N, since a linker polymer consists of a discrete number of monomers, the experimental linker length can never exactly match the optimal value. As can be seen in Fig.5a, a linker that is shorter than optimal leads to a significantly increased K_5, in particular for close-to-optimal values of d_{core}, a linker that is slightly longer than optimal only increases K_5 slightly. We conclude that in experimental ligand design, the linker should preferably be slightly longer than optimal, not shorter. Fig.5a also shows the experimental optimal dissociation constants K_5 for core sizes $d_{\text{core}} = 0.3$nm, 0.5 nm, 0.7 nm and 0.8 nm that correspond to the minimal values of K_5 with respect to linker length.[27,28] In agreement with the model predictions, K_5 remains nearly constant for core sizes smaller than 1nm and the drastic improvement of binding affinity for increasing core size was not reached in the experiments.

Multivalent Enhancement Diagram: The black horizontal line in Fig.5a denotes $K_5 = K_1/5 =$ 1 mM, for which the IC_{50} value of the pentavalent ligand is the same as of the monovalent ligand. From the crossing of this line with the prediction of K_5 for the multivalent ligand, we see that for

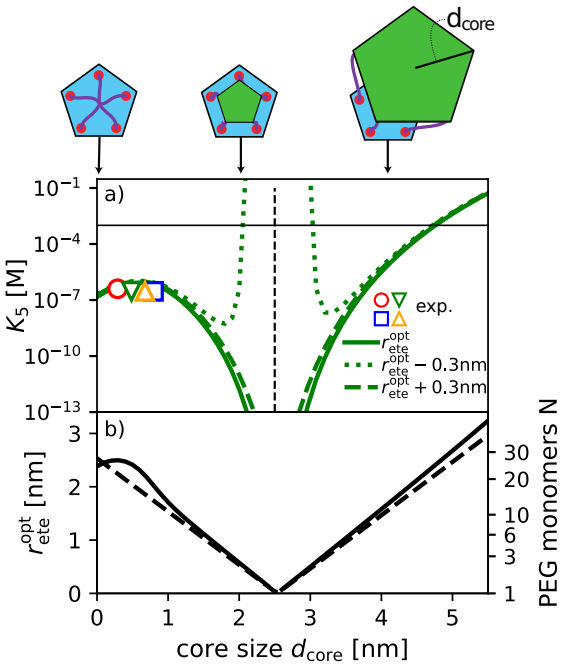

Figure 5: **Influence of ligand core size** d_{core}**:** a) Dissociation constant K_5 of a pentavalent ligand binding to cholera toxin as a function of d_{core}, optimal size match between ligand and receptor $d_{\text{core}} = d_{\text{rec}} = 2.5nm$ is indicated by a vertical dashed line. Schematic pictures are shown at the top. Results for optimal linker length (solid line) are compared with linkers shorter (dotted line) and longer than optimal (broken line). Experimental results for K_5 for optimal linker length are shown as colored symbols. The IC_{50} value of the monovalent ligand, $K_1/5$=1mM, is shown as a horizontal solid line. b) Optimal linker length $r_{\text{ete}}^{\text{opt}}$ (solid line). The difference between core size and receptor size, $|d_{\text{core}} - d_{\text{rec}}|$, is denoted by straight dashed lines.

a core size larger than d_{core} =4.6nm, the monovalent ligand binds more efficiently to the cholera receptor than the multivalent ligand, even when its linker length is optimized. This means that the monovalent dissociation constant K_1 is a crucial parameter which determines whether a multivalent ligand with a certain core size can be more efficient than its monovalent counterpart.

More generally, a multivalent ligand produces an α-fold binding enhancement compared to the monovalent ligand if the multivalent and monovalent dissociation constants satisfy the condition $\alpha K_n = K_1/n$. Using Eq.3 we obtain for the dependency of K_1 on the enhancement factor α the explicit expression

$$K_1 = (\alpha n)^{-\frac{1}{n-1}} \omega_{\text{LU}}^{\frac{-n}{n-1}} m^{\frac{n}{n-1}} C_1^{\frac{1}{n-1}}. \tag{6}$$

In Fig.6a we show Eq.6 in dependence of the ligand-receptor size ratio $d_{\text{core}}/d_{\text{rec}}$ for enhancement factors of $\alpha = 1, 10^3, 10^6, 10^9$ and for optimized linker length $r_{\text{ete}} = r_{\text{ete}}^{\text{opt}}$. We present results for trivalent ligands binding to the hemagglutinin receptor ($n = 3$, left panel), pentavalent ligands binding to the cholera toxin receptor ($n = 5$, middle panel), as well as heptavalent ligands binding

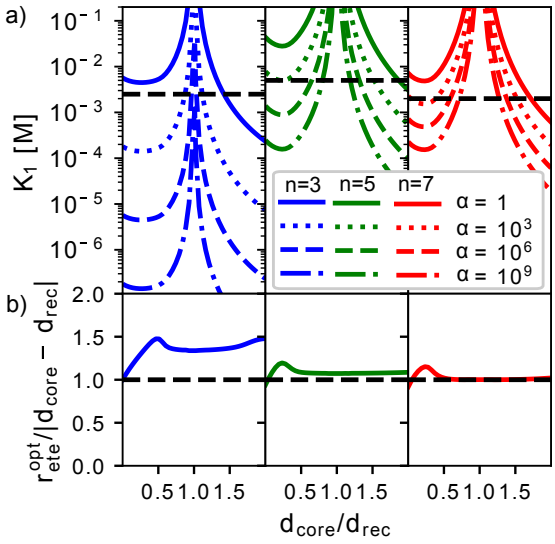

Figure 6: **Multivalent enhancement diagram:** a) Monovalent dissociation constant K_1 from Eq.6 required to reach multivalent enhancement factors $\alpha = 1, 10^3, 10^6, 10^9$ as a function of the ligand-receptor size ratio $d_{\rm core}/d_{\rm rec}$ for optimal linker length $r_{\rm ete}^{\rm opt}$ for trivalent ($n = 3$, left), pentavalent ($n = 5$, middle) and heptavalent ($n = 7$, right) receptor-ligand pairs. The experimental monovalent dissociation constants $K_1 = 2.5$mM ($n = 3$), $K_1 = 5$mM ($n = 5$) and $K_1 = 2$mM ($n = 7$) are shown as a horizontal broken lines. The angular restriction factor is set to $\omega_{\rm LU}$=0.06 (n=3), $\omega_{\rm LU}$=0.03 (n=5), $\omega_{\rm LU}$=0.06 (n=7). In accordance with the receptor structure in Fig.1a the number of binding pockets per receptor subunit m and the receptor size $d_{\rm rec}$ is set to m=1, d_{rec}=2.6nm (n=3), m=1, d_{rec}=2.5nm (n=5) and m=2, d_{rec}=3.5nm (n=7). b) Rescaled optimal linker length $r_{\rm ete}^{\rm opt}/|d_{\rm core} - d_{\rm rec}|$, the geometric limit $r_{\rm ete}^{\rm opt} = |d_{\rm core} - d_{\rm rec}|$) is denoted by dashed lines.

to the anthrax receptor ($n = 7$, right panel). The plots in Fig. 6a constitute enhancement diagrams of multivalent ligands, for a desired enhancement factor α and given ligand-receptor size ratio $d_{\rm core}/d_{\rm rec}$ the lines allow to determine the required monovalent dissociation constant K_1. The estimated values of the experimental monovalent dissociation constants $K_1 = 2.5$mM (hemagglutinin[13]), $K_1 = 5$mM (cholera toxin[27,28]) and $K_1 = 2$mM (anthrax[29]) are indicated by broken horizontal lines. For values of the monovalent dissociation constant K_1 above the solid line, which indicates the case $\alpha = 1$, a multivalent ligand is less efficient than its monovalent counterpart. For penta- and heptavalent ligands, we see that in order to reach an $\alpha = 10^6$-fold multivalent enhancement (broken line), the ligand core size must be in the range $2.1nm < d_{\rm core} < 4.9nm$ (for n=5) or $1.7nm < d_{\rm core} < 3.4nm$ (for n=7), respectively. To reach the same enhancement for hemagglutinin with sialic acid as a ligand unit, the core size must almost exactly match the optimal value $d_{\rm core} = d_{\rm rec}$, which would be very difficult to achieve in practice. If the linker length is off its optimal value, the restrictions on the core size are even more stringent (see Supporting

Information). The rescaled optimized linker length, $r_{\rm ete}^{\rm opt}/|d_{\rm core}-d_{\rm rec}|$, is shown as a function of $d_{\rm core}/d_{\rm rec}$ in Fig. 6b. In agreement with our results for the optimal linker length $r_{\rm ete}^{\rm opt}$ of a pentavalent ligand shown in Fig.5b, we find that $r_{\rm ete}^{\rm opt}$ is always slightly larger than the difference between core size and receptor size $|d_{\rm core}-d_{\rm rec}|$. The multivalent enhancement diagrams in Fig. 6a put very stringent constraints on the geometric design of multivalent ligands with a desired performance as quantified by the enhancement factor α. The monovalent dissociation constant K_1 turns out to be the limiting factor.

Conclusion

We present an analytic model for the binding affinity between multivalent ligand-receptor pairs that accounts for fluctuations of ligand core position and ligand core orientation as well as for conformational fluctuations of the polymeric linkers. Comparison with experimental multivalent binding data for pentavalent cholera ligands and heptavalent anthrax ligands is satisfactory and identifies the angular restriction between ligand units and linker polymers, quantified by the factor $\omega_{\rm LU}$, as a key ingredient of multivalent enhancement, which we believe is relevant also for multivalent binding in soft supramolecular structures, artificial self-assembling systems or self healing systems.[38–41] Our findings show that the highest gain in binding affinity is achieved for a ligand core size that matches the receptor size. In turn, a mismatch between core size and receptor size leads to a strong decrease of the binding affinity even for optimized linker length, this would allow multivalent ligands to discriminate between receptors of different size. The optimal linker length is slightly longer than needed to span the distance between receptor and core. The monovalent dissociation constant K_1 significantly influences the enhancement factor of an optimally designed multivalent ligand. We conclude that for the development of high affinity multivalent inhibitors against multivalent pathogens[3,42,43] the multivalent ligand geometry and the monovalent ligand unit binding affinity have to be balanced.

In our model we consider the valency of the ligands to precisely match the valency of the receptors, which is the prevalent scenario that is considered experimentally. Note however that Kitov *et al.*[21] designed a decavalent cholera toxin inhibitor. In future work it would therefore be interesting to generalize our model and to treat also the case of non-matching ligand and receptor valencies. We considered the idealized case where one multivalent ligand interacts with only one multivalent receptor, which corresponds to the limit of large spatial separation between neighboring multivalent receptors. For densely packed receptors a single multivalent ligand could bridge between different multivalent receptors, which would increase the number of binding patterns and therefore further strengthen the binding. For the meaningful modeling of such more complicated situations one would of course need to know the separation distribution between multivalent receptors.

Acknowlegement

This work was supported by the Deutsche Forschungsgemeinschaft within a grant from Sonderforschungsbereich (SFB) 765.

Supporting Information Available

The derivation of the multivalent dissociation constant and further discussions of the model are presented in the Supporting Information. This material is available free of charge *via* the Internet at http://pubs.acs.org.

References

[1] Nguyen, T. K. N.; Tran, V. M.; Sorna, V.; Eriksson, I.; Kojima, A.; Koketsu, M.; Loganathan, D.; Kjellen, L.; Dorsky, R. I.; Chien, C.-B.; Kuberan, B. Dimerized Glycosaminoglycan Chains Increase FGF Signaling during Zebrafish Development. *ACS Chem. Biol.* **2013**, *8*, 939–948.

[2] Satav, T.; Huskens, J.; Jonkheijm, P. Effects of Variations in Ligand Density on Cell Signaling. *Small* **2015**, *11*, 5184–5199.

[3] Levine, P. M.; Carberry, T. P.; Holub, J. M.; Kirshenbaum, K. Crafting Precise Multivalent Architectures. *Med. Chem. Commun.* **2013**, *4*, 493–509.

[4] Ribeiro-Viana, R.; Sanchez-Navarro, M.; Luczkowiak, J.; Koeppe, J. R.; Delgado, R.; Rojo, J.; Davis, B. G. Virus-Like Glycodendrinanoparticles Displaying Quasi-Equivalent Nested Polyvalency upon Glycoprotein Platforms Potently Block Viral Infection. *Nat. Commun.* **2012**, *3*.

[5] Wang, S.-K.; Liang, P.-H.; Astronomo, R. D.; Hsu, T.-L.; Hsieh, S.-L.; Burton, D. R.; Wong, C.-H. Targeting the Carbohydrates on HIV-1: Interaction of Oligomannose Dendrons with Human Monoclonal Antibody 2G12 and DC-SIGN. *Proc. Natl. Acad. Sci. USA* **2008**, *105*, 3690–3695.

[6] Wang, S.; Dormidontova, E. E. Selectivity of Ligand-Receptor Interactions between Nanoparticle and Cell Surfaces. *Phys. Rev. Lett.* **2012**, *109*, 238102.

[7] Hu, J.; Lipowsky, R.; Weikl, T. R. Binding Constants of Membrane-Anchored Receptors and Ligands Depend Strongly on the Nanoscale Roughness of Membranes. *Proc. Natl. Acad. Sci. USA* **2013**, *110*, 15283–15288.

[8] Fasting, C.; Schalley, C. A.; Weber, M.; Seitz, O.; Hecht, S.; Koksch, B.; Dernedde, J.; Graf, C.; Knapp, E.-W.; Haag, R. Multivalency as a Chemical Organization and Action Principle. *Angew. Chem. Int. Ed.* **2012**, *51*, 10472–10498.

[9] Cuesta, A. M.; Sainz-Pastor, N.; Bonet, J.; Oliva, B.; Alvarez-Vallina, L. Multivalent Antibodies: When Design Surpasses Evolution. *Trends Biotechnol.* **2010**, *28*, 355–362.

[10] Branson, T. R.; Turnbull, W. B. Bacterial Toxin Inhibitors Based on Multivalent Scaffolds. *Chem. Soc. Rev.* **2013**, *42*, 4613–4622.

[11] Stencel-Baerenwald, J. E.; Reiss, K.; Reiter, D. M.; Stehle, T.; Dermody, T. S. The Sweet Spot: Defining Virus-Sialic Acid Interactions. *Nat Rev Microbiol* **2014**, *12*, 739–749.

[12] Mammen, M.; Choi, S.; Whitesides, G. Polyvalent Interactions in Biological Systems: Implications for Design and Use of Multivalent Ligands and Inhibitors. *Angew. Chem. Int. Ed.* **1998**, *37*, 2755–2794.

[13] Lees, W.; Spaltenstein, A.; Kingerywood, J.; Whitesides, G. Polyacrylamides Bearing Pendant Alpha-Sialoside Groups Strongly Inhibit Agglutination of Erythrocytes by Influenza-A Virus - Multivalency and Steric Stabilization of Particulate Biological-Systems. *J. Med.Chem.* **1994**, *37*, 3419–3433.

[14] Deniaud, D.; Julienne, K.; Gouin, S. G. Insights in the Rational Design of Synthetic Multivalent Glycoconjugates as Lectin Ligands. *Org. Biomol. Chem.* **2011**, *9*, 966–979.

[15] Xu, H.; Shaw, D. E. A Simple Model of Multivalent Adhesion and Its Application to Influenza Infection. *Biophys. J.* **2016**, *110*, 218–233.

[16] Martinez-Veracoechea, F.; Frenkel, D. Designing Super Selectivity in Multivalent Nano-Particle Binding. *Proc. Natl. Acad. Sci. USA* **2011**, *108*, 10963–10968.

[17] Dubacheva, G. V.; Curk, T.; Auzely-Velty, R.; Frenkel, D.; Richter, R. P. Designing Multivalent Probes for Tunable Superselective Targeting. *Proc. Natl. Acad. Sci. USA* **2015**, *112*, 5579–5584.

[18] Wittmann, V.; Pieters, R. J. Bridging Lectin Binding Sites by Multivalent Carbohydrates. *Chem. Soc. Rev.* **2013**, *42*, 4492–4503.

[19] Zuilhof, H. Fighting Cholera One-on-One: The Development and Efficacy of Multivalent Cholera-Toxin-Binding Molecules. *Acc. Chem. Res.* **2016**, *49*, 274–285.

[20] Bhatia, S.; Dimde, M.; Haag, R. Multivalent Glycoconjugates as Vaccines and Potential Drug Candidates. *Med. Chem. Commun.* **2014**, *5*, 862–878.

[21] Kitov, P.; Sadowska, J.; Mulvey, G.; Armstrong, G.; Ling, H.; Pannu, N.; Read, R.; Bundle, D. Shiga-Like Toxins are Neutralized by Tailored Multivalent Carbohydrate Ligands. *Nature* **2000**, *403*, 669–672.

[22] Mulder, A.; Huskens, J.; Reinhoudt, D. Multivalency in Supramolecular Chemistry and Nanofabrication. *Org. Biomol. Chem.* **2004**, *2*, 3409–3424.

[23] World Health Organization, Fact Sheet Nr. 211, March 2014. 2014.

[24] Kadam, R. U.; Wilson, I. A. Structural Basis of Influenza Virus Fusion Inhibition by the Antiviral Drug Arbidol. *Proc. Natl. Acad. Sci. USA* **2017**, *114*, 206–214.

[25] Waldmann, M.; Jirmann, R.; Hoelscher, K.; Wienke, M.; Niemeyer, F. C.; Rehders, D.; Meyer, B. A Nanomolar Multivalent Ligand as Entry Inhibitor of the Hemagglutinin of Avian Influenza. *J. Am. Chem. Soc.* **2014**, *136*, 783–788.

[26] Hunter, C. A.; Anderson, H. L. What is Cooperativity? *Angew. Chem. Int. Ed.* **2009**, *48*, 7488–7499.

[27] Zhang, Z.; Liu, J.; Verlinde, C.; Hol, W.; Fan, E. Large Cyclic Peptides as Cores of Multivalent Ligands: Application to Inhibitors of Receptor Binding by Cholera Toxin. *J. Org. Chem.* **2004**, *69*, 7737–7740.

[28] Zhang, Z.; Pickens, J.; Hol, W.; Fan, E. Solution- and Solid-Phase Syntheses of Guanidine-Bridged, Water-Soluble Linkers for Multivalent Ligand Design. *Org. Lett.* **2004**, *6*, 1377–1380.

[29] Joshi, A.; Kate, S.; Poon, V.; Mondal, D.; Boggara, M. B.; Saraph, A.; Martin, J. T.; McAlpine, R.; Day, R.; Garcia, A. E.; Mogridge, J.; Kane, R. S. Structure-Based Design of a Heptavalent Anthrax Toxin Inhibitor. *Biomacromolecules* **2011**, *12*, 791–796.

[30] Liese, S.; Netz, R. R. Influence of Length and Flexibility of Spacers on the Binding Affinity of Divalent Ligands. *Beilstein J. Org. Chem.* **2015**, *11*, 804–816.

[31] Diestler, D. J.; Knapp, E. W. Statistical Mechanics of the Stability of Multivalent Ligand-Receptor Complexes. *J. Phys. Chem. C* **2010**, *114*, 5287–5304.

[32] Soler, M. A.; Fortuna, S. F. Influence of Linker Flexibility on the Binding Affinity of Bidentate Binders. *J. Phys. Chem. B* **2017**, *16*, 3918?3924.

[33] Lo Conte, M.; Staderini, S.; Chambery, A.; Berthet, N.; Dumy, P.; Renaudet, O.; Marra, A.; Dondoni, A. Glycoside and Peptide Clustering Around the Octasilsesquioxane Scaffold via Photoinduced Free-Radical Thiolene Coupling. The Observation of a Striking Glycoside Cluster Effect. *Org. Biomol. Chem.* **2012**, *10*, 3269–3277.

[34] Vonnemann, J.; Sieben, C.; Wolff, C.; Ludwig, K.; Boettcher, C.; Herrmann, A.; Haag, R. Virus Inhibition Induced by Polyvalent Nanoparticles of Different Sizes. *Nanoscale* **2014**, *6*, 2353–2360.

[35] Huskens, J.; Mulder, A.; Auletta, T.; Nijhuis, C.; Ludden, M.; Reinhoudt, D. A Model for Describing the Thermodynamics of Multivalent Host-Guest Interactions at Interfaces. *J. Am. Chem. Soc.* **2004**, *126*, 6784–6797.

[36] Liese, S.; Gensler, M.; Krysiak, S.; Schwarzl, R.; Achazi, A. J.; Paulus, B.; Hugel, T.; Rabe, J. P.; Netz, R. R. Hydration Effects Turn a Highly Stretched Polymer from an Entropic into an Energetic Spring. *ACS Nano* **2017**, *11*, 702–712.

[37] Fan, E.; Zhang, Z.; Minke, W.; Hou, Z.; Verlinde, C.; Hol, W. High-Affinity Pentavalent Ligands of Escherichia Coli Heat-Labile Enterotoxin by Modular Structure-Based Design. *J. Am. Chem. Soc.* **2000**, *122*, 2663–2664.

[38] Cordier, P.; Tournilhac, F.; Soulie-Ziakovic, C.; Leibler, L. Self-Healing and Thermoreversible Rubber from Supramolecular Assembly. *Nature* **2008**, *451*, 977–980.

[39] Harada, A.; Takashima, Y.; Nakahata, M. Supramolecular Polymeric Materials via Cyclodextrin-Guest Interactions. *Acc. Chem. Res.* **2014**, *47*, 2128–2140.

[40] Hamley, I. Nanotechnology with Soft Materials. *Angew. Chem. Int. Ed.* **2003**, *42*, 1692–1712.

[41] Curk, T.; Dobnikar, J.; Frenkel, D. Rational Design of Molecularly Imprinted Polymers. *Soft Matter* **2016**, *12*, 35–44.

[42] Diezmann, F.; von Kleist, L.; Hauckeb, V.; Seitz, O. Probing Heterobivalent Binding to the Endocytic AP-2 Adaptor Complex by DNA-Based Spatial Screening. *Org. Biomol. Chem.* **2015**, *13*, 8008–8015.

[43] Zacco, E.; Anish, C.; Martin, C. E.; von Berlepsch, H.; Brandenburg, E.; Seeberger, P. H.; Koksch, B. A Self-Assembling Peptide Scaffold for the Multivalent Presentation of Antigens. *Biomacromolecules* **2015**, *16*, 2188–2197.

Graphical TOC Entry